Journal of Inflammation Research

Dovepress
Taylor & Francis Group

Open Access Full Text Article

ORIGINAL RESEARCH

SULF1's Role in Endothelial Senescence and Atherosclerosis: Insights from Single-Cell and Bulk Transcriptomics

Meng-Ting Jiang[1,*], Shi-Lei Wan[1,*], Xiang-Yu Shen[1,*], Zhong-Bai Zhang[1], Zhi-Qing He[1], Yang-Xi Hu[1–4], Chun Liang[1]

[1]Department of Cardiology, Second Affiliated Hospital of Naval Medical University, Shanghai Cardiovascular Institute of Integrative Medicine, Shanghai, 200003, People's Republic of China; [2]Department of Cardiology, Daping Hospital, Army Medical University, Chongqing, 400042, People's Republic of China; [3]Key Laboratory of Geriatric Cardiovascular and Cerebrovascular Disease Research, Ministry of Education of China, Chongqing, 400042, People's Republic of China; [4]Chongqing Key Laboratory for Hypertension Research, Chongqing Cardiovascular Clinical Research Center, Chongqing Institute of Cardiology, Chongqing, 400042, People's Republic of China

*These authors contributed equally to this work

Correspondence: Chun Liang, Department of Cardiology, Second Affiliated Hospital of Naval Medical University, Shanghai Cardiovascular Institute of Integrative Medicine, 415 Fengyang Road, Shanghai, 200003, People's Republic of China, Tel +86-21-81885291, Email chunliangliang1985@163.com; Yang-Xi Hu, Department of Cardiology, Daping Hospital, Army Medical University, 10 Changjiang Branch Road, Chongqing, 400042, People's Republic of China, Tel +86-21-81512526, Email yxhu@smmu.edu.cn

Background: Endothelial cells (ECs) senescence has emerged as a critical factor in the pathogenesis of atherosclerosis, contributing to vascular aging and plaque formation. However, the molecular mechanisms underlying endothelial senescence in atherosclerosis remain poorly understood.

Methods: Single-cell RNA sequencing (scRNA-seq) data from atherosclerotic core plaques and adjacent normal tissues were analyzed using the Seurat package to identify cell subpopulations and senescence markers. RNA-seq data from early and late atherosclerotic plaques were used for differential gene expression analysis. Subsequently, the candidate gene was identified and validated in the atherosclerotic plaques of *ApoE*$^{-/-}$ mice and ox-LDL-treated human aortic ECs (HAECs) through siRNA knockdown, Western blot, RT-qPCR, and β-galactosidase staining in vitro.

Results: Single-cell analysis revealed elevated levels of senescence markers in ECs within atherosclerotic plaques. Combined with bulk RNA-seq analysis, *SULF1* was identified as a key gene associated with EC senescence. Increased *Sulf1* expression was uncovered in the ECs of atherosclerotic plaques in high-fat-fed *ApoE*$^{-/-}$ mice. In vitro, *SULF1* expression was found significantly upregulated in senescent HAECs. Knockdown of *SULF1* reversed ox-LDL-induced senescence in HAECs, as shown by reduced expression of senescence markers and improved cell migration in wound healing assays.

Conclusion: This study highlights the critical role of endothelial senescence in atherosclerosis and identifies *SULF1* as a key contributor to endothelial senescence and atherogenesis. Targeting *SULF1* may be a potential therapeutic strategy for mitigating EC senescence and atherosclerosis.

Keywords: atherosclerosis, endothelial senescence, single-cell RNA sequencing, RNA sequencing, *SULF1*

Introduction

Atherosclerosis continues to be the predominant contributor to global cardiovascular disease burden and death rates.[1,2] The disease pathogenesis involves multiple interrelated mechanisms, encompassing intricate crosstalk between endothelial cells, immune components, lipid particles, and vascular wall elements.[3] At the core of these processes lies the endothelium - a single-cell layer covering the luminal surface of blood vessels that serves essential functions in preserving vascular equilibrium.[4] Originally regarded as simply an passive barrier, the endothelium is currently recognized as a metabolically active regulator of both vascular physiology and pathology. This cellular layer represents

Received: 18 June 2025
Accepted: 6 December 2025
Published: 16 December 2025

the principal interface between circulating blood and vascular tissues, playing fundamental roles in modulating blood vessel diameter, inflammatory responses, thrombosis, and angiogenesis.[5]

Emerging evidence indicates that impaired endothelial cell (EC) function serves as a primary trigger for atherosclerotic lesion development, with growing recognition of cellular senescence as a key pathological mechanism in this process.[6–8] The senescent endothelial phenotype, marked by permanent proliferative arrest and modified secretory activity, has been established as a fundamental contributor to vascular aging and atherogenesis.[9,10] Notably, senescent ECs maintain a persistent pro-inflammatory secretory state that facilitates immune cell infiltration, foam cell generation, and extracellular matrix accumulation - characteristic features of developing atherosclerotic lesions.[11] Despite these advances, the precise cellular mechanisms and molecular pathways governing endothelial senescence in atherosclerosis remain incompletely understood.

Sulfatase 1 (SULF1) is an enzyme localized on the cell surface that edits the sulfation pattern of heparan sulfate proteoglycans (HSPGs) by removing 6-O-sulfate groups. This activity fundamentally alters the binding capacity of HSPGs for a myriad of signaling molecules, such as growth factors and cytokines, thereby functioning as a critical master regulator of key signaling pathways.[12,13] Research indicates that SULF1 expression in endothelial cells is upregulated by pro-atherogenic processes like Endothelial-to-Mesenchymal Transition (EndMT), placing it within a key pathological pathway.[14] Crucially, single-cell transcriptomic studies reveal that a specific $SULF1^{+}$ endothelial cell subset is markedly enriched in the carotid plaques of symptomatic patients who have experienced cerebrovascular events.[15] However, the specific relationship between SULF1, atherosclerosis, and endothelial cell senescence remains unclear. In this study, the role of endothelial senescence in the process of atherosclerosis was described at two dimensions. Spatially, at the single-cell resolution, endothelial senescence markers were found significantly elevated in atherosclerotic core plaques. Temporally, key regulators were identified through a differential analysis performed using the bulk RNA sequencing (RNA-seq) data between early and late atherosclerotic plaques. Taken together, *SULF1* was screened out and validated to be a significant contributor in endothelial senescence and atherogenesis.

Materials and Methods

Single-Cell RNA Sequencing (ScRNA-Seq) Transcriptomics

The data utilized in this study were obtained from the GEO database under the accession number GSE159677.[16] The Seurat package enabled object creation and removal of substandard cells during routine preprocessing steps. Threshold-based filtering was implemented to calculate gene and cell quantities along with mitochondrial percentage, eliminating genes present in less than 3 cells and cells containing fewer than 200 detectable genes. Only genes identified in a minimum of 200 cells were preserved, whereas cells exhibiting either less than 300 detected genes or elevated mitochondrial proportions (exceeding 15%) were discarded. Cellular normalization was achieved through UMI count scaling at 10,000× magnification. Subsequent to logarithmic conversion, the ScaleData functionality within Seurat (v4.0.2) was employed.

RNA-Seq Analysis

The GEO Public Database archives contain experimental data contributed by researchers globally and are accessible via https://www.ncbi.nlm.nih.gov/geo/. Data from GEO accession GSE28829 were downloaded and included gene expression in early and late atherosclerotic plaques in human carotid arteries, encompassing 16 late and 13 early plaque cases.[17]

This research qualifies for an exemption from further institutional ethics review, in accordance with Article 32 of the "Measures for the Ethical Review of Life Science and Medical Research Involving Human Subjects" (effective February 18, 2023) of the People's Republic of China. Specifically, our study falls under the exemption clause for research that: "research conducted using publicly available data obtained legally, or information collected through non-intrusive methods such as observation that does not involve personal privacy". The GEO database is a publicly accessible resource, and our use of its anonymized data strictly adhered to its access policies and terms of use. The research does not involve any new data collection from human subjects and poses no risk to personal privacy.

Cell Subpopulation Analysis, Clustering, and Preliminary Cell Type Identification

The analytical workflow utilized corrected and normalized data metrics as input. Variable gene selection prioritized the most highly variable 2000 transcripts for dimensionality reduction through principal component analysis (PCA), with retention of the initial 20 principal components for subsequent dimensional reduction visualization via either Uniform Manifold Approximation and Projection (UMAP) or t-distributed Stochastic Neighbor Embedding (t-SNE). Cellular subpopulation identification was achieved through implementation of the FindClusters algorithm within the Seurat environment (cluster resolution parameter = 0.5), yielding 15 discrete cell populations.

Technical artifacts arising from batch-to-batch variation and inter-individual heterogeneity were addressed through application of the Harmony integration method. Differential gene expression patterns across identified clusters were characterized using the FindAllMarkers tool with stringent thresholds: minimum percentage expression (min.pct) = 0.15, minimum log2 fold-change (logfc.threshold) = 0.15, and exclusive consideration of positively expressed markers (only.pos = TRUE). Statistical significance was assessed through Wilcoxon signed-rank testing with Benjamini-Hochberg false discovery rate adjustment, with corrected *p*-values informing all comparative evaluations.

Functional Enrichment and Gene Set Enrichment Analysis

Gene ontology and pathway enrichment investigations were conducted employing the clusterProfiler software tool (v4.7.1.2), specifically examining Kyoto Encyclopedia of Genes and Genomes (KEGG) biological routes. Metabolic and signaling pathways demonstrating Benjamini-Hochberg corrected *p*-values below the 0.05 threshold were deemed statistically significant in relation to the identified differentially expressed genes (DEGs, Supplementary Table 3).

Heatmap Analysis

Gene expression patterns were visualized through heatmap representations, where experimental samples were organized on the x-axis while gene identifiers were displayed on the y-axis. For dot plot generation, unprocessed RNA quantification values were proportionally adjusted to optimize graphical interpretation, enabling effective evaluation of transcriptional variation between discrete cellular subsets. The integrated visualization approach combining both heatmap and dot plot methodologies offers an exhaustive analytical framework for examining transcriptional profiles and their heterogeneity among diverse cell populations.

Pseudotime Analysis

To investigate cellular developmental pathways, pseudotemporal ordering was conducted using Monocle2 software (release 2.26.0).[18] For this analysis, transcripts exhibiting average expression values greater than 0.1 were initially selected. Subsequent gene filtering was performed through the differentialGeneTest module, implementing a rigorous significance cutoff of $q<0.01$ to eliminate transcripts unsuitable for trajectory construction. Data dimensionality reduction was achieved by implementing the reduceDimension computational module incorporating the DDRTree manifold learning approach. All computational processes utilized standard parameter configurations. The final cellular pseudotime alignment was generated via the orderCells analytical routine.

Animal Experiments

Male C57BL/6 mice aged six weeks were procured from Gem Pharmatech (Nanjing, China) and acclimatized under controlled environmental conditions (12-hour photoperiod, 22–25°C ambient temperature, 45–55% relative humidity). Following a 7-day adaptation period with standard rodent chow, $ApoE^{-/-}$ mice received an atherogenic diet (21% lipid content with 0.15% cholesterol; Keao Xieli Feed Co., Beijing China) for 24 weeks to establish atherosclerotic lesions, with wild-type littermates maintained on normal chow as controls. Aortic tissue specimens were harvested upon study completion for subsequent histopathological analysis.

Female 8-week-old mice were used in this study, with the experimental group comprised $ApoE^{-/-}$ mice, while the control group consisted of C57BL/6J mice. All mice were purchased from Shanghai Slac laboratory animal Co., Ltd. and housed under specific pathogen-free (SPF) conditions in a controlled environment (temperature: 22 ± 1°C; humidity: 50 ± 15%; 12-hour light/dark cycle). Following a 2-week adaptive feeding on standard chow, the mice were fed a Western

diet (supplemented with 0.15% cholesterol; Jiangsu Xietong Medicine Bioengineering Co., Ltd., China) for 10 weeks. Subsequently, right carotid artery tissues were harvested and processed for histological staining.

All experimental protocols were performed in compliance with institutional guidelines for laboratory animal care and were approved by the Institutional Animal Care and Use Committee at Shanghai Changzheng Hospital. Uniform housing and handling conditions were maintained throughout the study period to minimize environmental variability.

Immunofluorescence

The specimens were initially preserved in a 4% paraformaldehyde solution containing 4% sucrose, followed by cryoprotection in 30% sucrose solution. Paraffin-embedded sections were processed through sequential immunostaining procedures. Initially, antigen retrieval was performed, and nonspecific binding sites were blocked using a solution containing 0.1% Triton X-100 and 5% normal goat serum for 60 minutes at ambient temperature. The sections were then exposed to primary antibodies against CD31 (11265-1-AP, Proteintech, Wuhan, China) for 16 hours at 4°C, followed by appropriate species-specific secondary antibodies conjugated with either Alexa Fluor 488 or 594 (gb2AF488, Proteintech, Wuhan, China) for 60 minutes at room temperature. Subsequently, the same sections underwent additional immunostaining with SULF1 antibodies (27438-1-AP, Proteintech, Wuhan, China) using identical blocking and secondary antibody incubation conditions. Cellular nuclei were visualized using 4',6-diamidino-2-phenylindole (DAPI, 28718–90-3, Solarbio, Beijing, China) mounting medium.

Cell Culture and Drug Treatment

Primary human aortic endothelial cells (HAECs; QuiCell Biotech, Shanghai, China) were maintained in specialized endothelial growth medium (QuiCell-Pri-8003, QuiCell Biotech, Shanghai, China) under standard culture conditions (37°C, 5% CO_2, humidified atmosphere). Cells from passages 3–6 were utilized for experimental procedures. To simulate atherosclerotic conditions in vitro, confluent HAEC monolayers were treated with 50 μg/mL oxidized LDL (ox-LDL) for 24 hours prior to analysis.

Small Interfering RNA (SiRNA) Transfection

Gene silencing experiments were performed using *SULF1*-specific small interfering RNA (siRNA) and scrambled control siRNA (scRNA), both commercially obtained from RiboBio (Huzhou, China). Transfection of HAECs was carried out following standardized protocols with Lipofectamine 3000 transfection reagent (L3000075, Thermo Fisher Scientific, Waltham, MA, USA). Briefly, at 70–90% confluency, cells were exposed to the siRNA-lipid complexes for 6 hours, followed by replacement with complete endothelial cell growth medium for 48 hours. Successful gene knockdown was verified at both transcriptional and protein levels using reverse transcription quantitative PCR (RT-qPCR) and Western blot, respectively.

Protein Preparation and Western Blotting

Cellular protein extracts were obtained from HAECs through lysis in RIPA buffer containing protease inhibitors, followed by protein quantification via bicinchoninic acid method. Equal amounts of protein (30 μg per lane) were separated electrophoretically on 10% SDS-polyacrylamide gels under reducing conditions and then transferred to PVDF membranes (IEVH85R, Merck KGaA, Darmstadt, Germany) using semi-dry transfer apparatus.

For immunoblotting analysis, membranes were incubated with specific primary antibodies against SULF1 (27438-1-AP, Proteintech, Wuhan, China), p16 (AB51243, Abcam, Cambridge, UK), p21 (AB109520, Abcam, Cambridge, UK), p53 (AB131442, Abcam, Cambridge, UK) and GAPDH (AB181602, Abcam, Cambridge, UK) (all at 1:1000 dilution) for 16 hours at 4°C, then exposed to horseradish peroxidase-conjugated secondary antibodies (1:10,000 dilution, 511203, Zenbio, Chengdu, China) for 60 minutes at ambient temperature. Protein-antibody complexes were visualized by enhanced chemiluminescence detection system, using GAPDH expression as internal reference for data normalization. Band detection and densitometric quantification were carried out using FluorChem E digital imaging system and ImageJ analysis software respectively, with all target protein signals normalized to corresponding GAPDH bands.

RNA Extraction and RT-qPCR

RNA extraction from processed HAEC specimens was conducted with TRIzol reagent (15596018CN, Thermo Fisher Scientific, Waltham, USA). Subsequent to isolation, RNA templates were converted to cDNA through reverse transcription utilizing a PrimeScript RT kit featuring integrated genomic DNA elimination (R026A, Takara Bio, Otsu, Japan). Real-time PCR amplification was executed using SYBR Green-based detection chemistry following the supplier's recommended procedures. Oligonucleotide primer sets targeting specific genes are provided in Supplementary Table 1. Expression levels were determined through comparative CT ($2^{-\Delta\Delta CT}$) analysis for relative quantification.

Senescence-Associated β-Galactosidase (SA β-Gal) Staining

Senescence status in human aortic endothelial cells (HAECs) was assessed by measuring senescence-associated β-galactosidase (SA-β-gal) enzymatic activity (RG0039, Beyotime, Shanghai, China). Cells were seeded into 6-well plates and cultured to full confluency prior to experimental procedures. After fixation, cell monolayers were incubated with SA-β-gal staining reagent under controlled conditions (37°C, non-CO_2 environment) for an overnight period (16–18 h). For quantitative analysis, phase-contrast microscopic images were captured from multiple regions per well, followed by counting of SA-β-gal-positive cells in 10 randomly chosen microscopic fields at 10× total magnification.

Scratch Wound Assay

Cell migratory potential was assessed through a well-established wound closure assay. HAECs were plated in 12-well plates at 2×10^5 cells/well (triplicate wells per condition) and grown to form confluent monolayers. Mechanical wounding was performed with a sterile 10 μL pipette tip to generate consistent linear defects, after which the wells were rinsed three times with phosphate-buffered saline to clear detached cellular debris. Wound areas were documented by phase-contrast microscopy at baseline (0 hour) and following 24 hours of culture. Migration capacity was quantified by calculating the relative wound closure percentage according to the equation: Wound closure (%) = $[(A_0 - A_{24})/A_0] \times 100$, where A_0 represents the initial wound area and A_{24} denotes the remaining open area after 24 hours.

Statistical Analyses

All statistical computations were executed utilizing Seurat (v4.0.2) implemented in R programming language (v4.2.0), with additional analyses performed in SPSS (v22.0). Bivariate associations were examined through Spearman's rank-order correlation coefficient estimation. Time-to-event data were evaluated via Kaplan-Meier survival analysis incorporating Log rank test comparisons. For non-normally distributed variables, Kruskal–Wallis testing was initially applied, followed by pairwise Wilcoxon rank-sum examinations incorporating Benjamini-Hochberg adjustment for multiple hypothesis testing.

Data derived from three independent experimental replicates are expressed as arithmetic mean ± standard deviation. Multigroup comparisons employed one-way ANOVA with least significant difference post hoc analysis when indicated. Intergroup differential analysis was performed using two-tailed Student's *t*-tests assuming variance homogeneity. The predetermined threshold for statistical significance was established at $p < 0.05$ for all inferential analyses.

Detailed information of the reagents used in this study could be found in Supplementary Table 2.

Results

ECs Senescence Significantly Contributes to Atherosclerosis

The pathogenesis of atherosclerosis encompasses complex interactions between inflammatory processes, extracellular matrix reorganization, and cellular phenotype switching (CTD), presenting significant challenges for precise mechanistic characterization. We analyzed single-cell transcriptional profiles from fully calcified atheromatous core (AC) lesions and anatomically matched proximal adjacent (PA) reference tissues obtained during carotid endarterectomy procedures from three clinical cases. Cellular yields averaged around 13,000 cells per AC specimen and 5000 cells per PA control sample per patient. Technical variations across scRNA-seq datasets from AC and PA samples were harmonized using the batch correction Harmony algorithm (Figure 1A). Following quality control, approximately 50,000 high-quality cellular

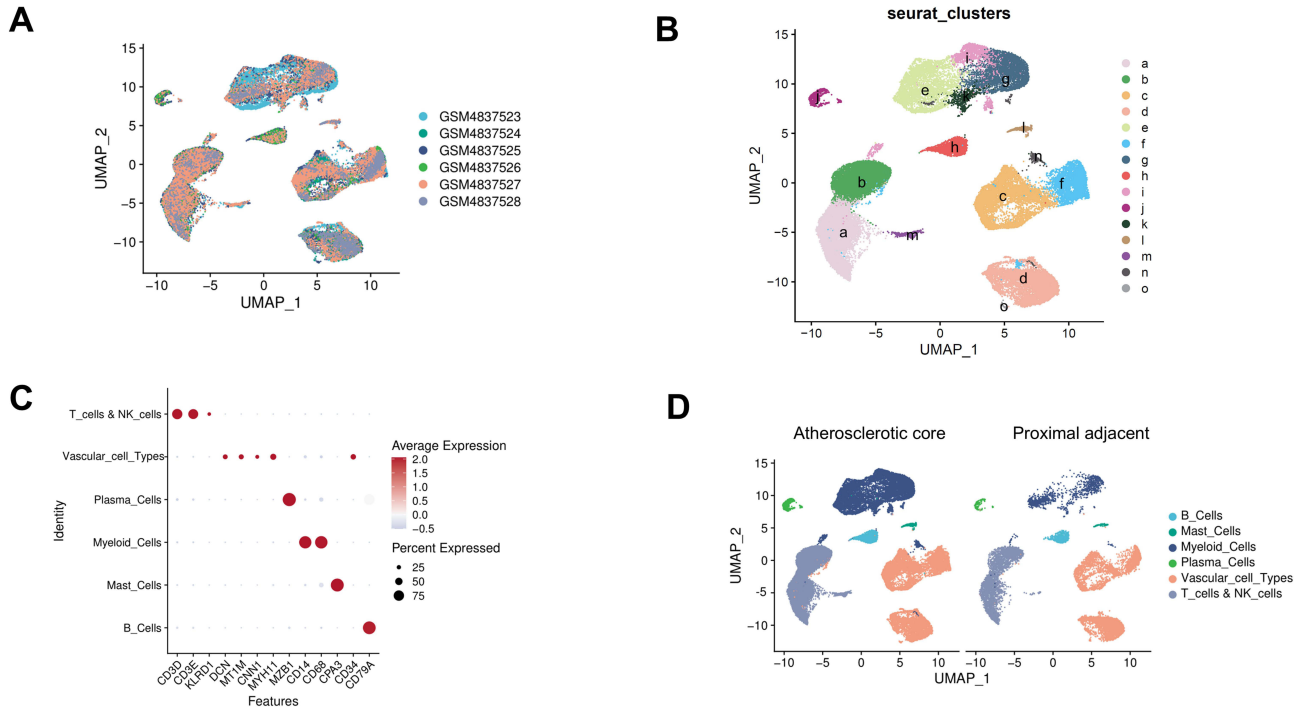

Figure 1 Data processing and cell type definition. (**A**) UMAP plot illustrating the distribution of cells within the GSE159677 dataset. (**B**) UMAP dimensionality reduction delineating the clusters. Individual cells are represented by dots, with colors indicating distinct cell populations. (**C**) A dot plot depicting six major cell types (T cells, NK cells, stromal cells, myeloid cells, mast cells, and B cells) and their marker genes. The size of each dot corresponds to the proportion of cells expressing a particular gene, whereas the color intensity reflects the level of gene expression. (**D**) UMAP plot highlighting the distribution of cell types between the atherosclerotic core (AC) plaques and proximal adjacent (PA) groups.

transcriptomes were included for downstream bioinformatic analysis, yielding 15 transcriptionally distinct clusters that mapped to seven principal cellular categories (Figure 1B). These subtypes were identified based on the expression of classic single-cell markers. B cells are indicated by *CD79A* expression, mast cells by *CPA3*, myeloid cells by the presence of *CD14* and *CD68*, and plasma cells by *MZB1*. Vascular cell types were identified through the expression of *DCN, MT1M, CNN1, MYH11*, and *CD34*, while T cells and NK cells were labeled with *CD3D* and *CD3E* (Figure 1C). We also performed quality control and cell annotation of the data including quantitative metrics of RNA features, organelle content, and an extensive *CD* marker profile (Supplementary Figure 1). While all six major cell types were identified in both the PA and AC groups, notable variations in their levels of infiltration were found. This discrepancy may correspond to the varying stages of CTD progression. A significantly greater proportion of vascular cell types was observed in the AC group than in the control group, indicating a potential role for these cells, including the vascular endothelium, in the progression of CTD (Figure 1D).

In our research, Single cells were segregated into nine distinct clusters (Figure 2A). We delineated three vascular cell subtypes based on marker gene expression: smooth muscle cells, ECs, and fibroblasts. Specifically, *ATCA2, TAGLN*, and *MYL9* gene signatures were used to distinguish smooth muscle cells, while *EDN1* and *EDSCR* were used for EC identification, and *DCN* and *COL1A2* were used for fibroblast characterization (Figure 2B–D). The t-SNE plot showed that the distribution of the three main cell types in different samples was significantly different (Figure 2E). Notably, ECs within the AC group presented characteristics indicative of senescence, as indicated by elevated *S100A4* expression in AC tissue relative to that in normal tissue (Figure 2F). These findings indicate a key role of ECs senescence in atherosclerosis.

SULF1 is a Key Gene Affecting Vascular Endothelial Senescence

To identify the key genes affecting endothelial senescence, we conducted an analysis of transcriptomic data to identify the genes contributing to the progression of human atherosclerotic plaques from early to advanced stages, denoted as

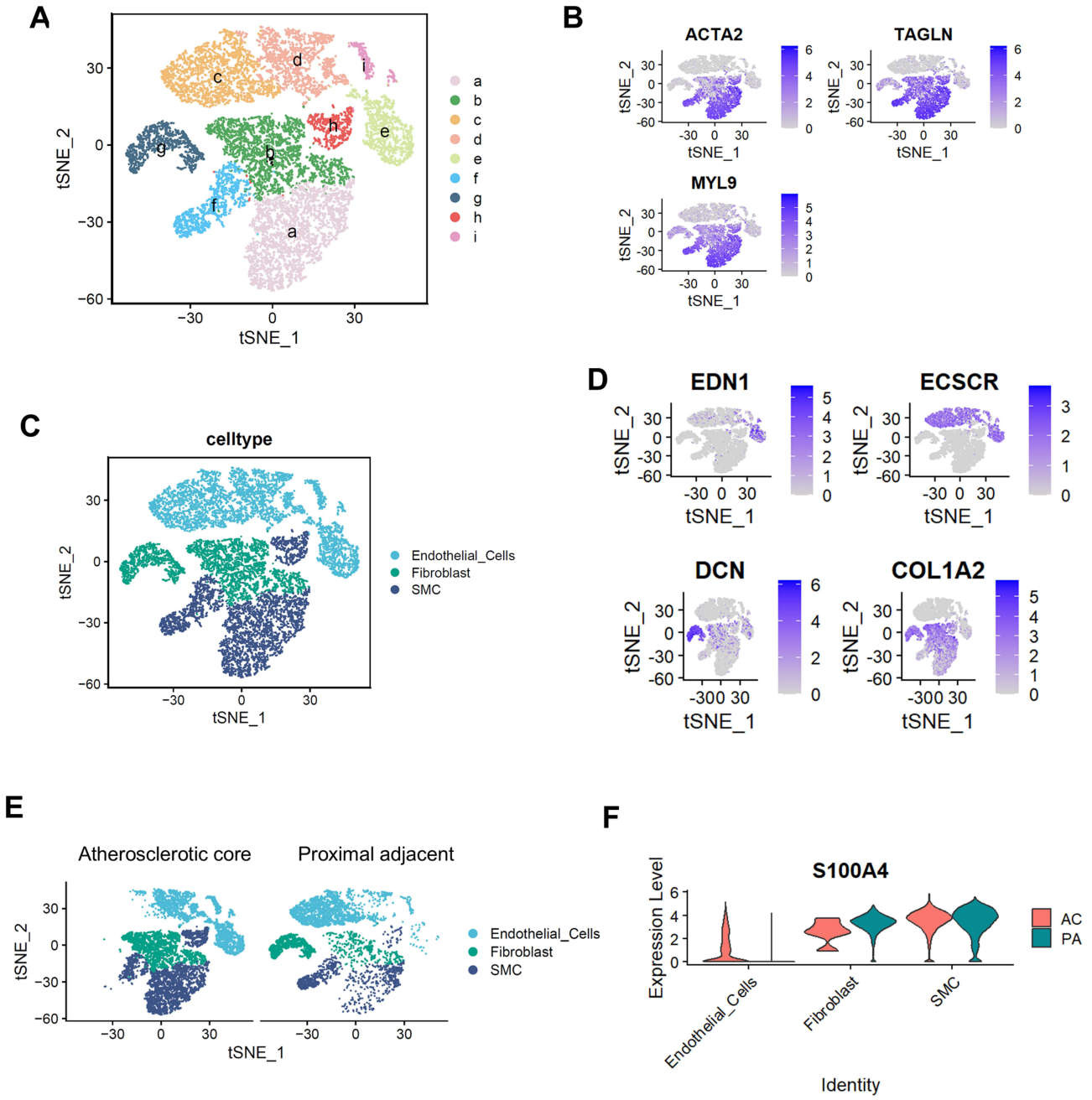

Figure 2 Endothelial senescence occurs in atherosclerotic plaques. (**A**) Single cells were segregated into nine distinct clusters. (**B**) Individual cells in tSNEs are colored according to average expression of smooth muscle cell markers. (**C**) t-SNE visualization of atherosclerosis stromal scRNA-seq profiles. (**D**) Individual cells in t-SNEs are colored according to average expression of fibroblasts and endothelial cells markers. (**E**) t-SNE plots displaying the distribution of the three major cell types in different samples. (**F**) Violin plot demonstrating the expression levels of *S100A4* in atherosclerotic core (AC) plaques and proximal adjacent (PA) vascular tissues.

Early and Advanced, respectively. PCA revealed a distinct separation between groups Early and Advanced, indicating significant transcriptional differences existed in early atherosclerotic plaques (Figure 3A). Compared with patients with early-stage atherosclerosis, patients with advanced-stage atherosclerosis presented senescence-associated characteristics, including elevated expression of *Cyclin dependent kinase inhibitor 2A* (*CDKN2A*, or *P16*), a marker indicative of cellular senescence (Figure 3B), and the activation of cellular senescence pathways (Figure 3C). A heatmap, which depicts the expression profiles of senescence-related genes from the KEGG database across different subgroups, revealed that the expression of these senescence-associated genes was significantly greater in the Advanced group (Figure 3D).

https://doi.org/10.2147/JIR.S544852

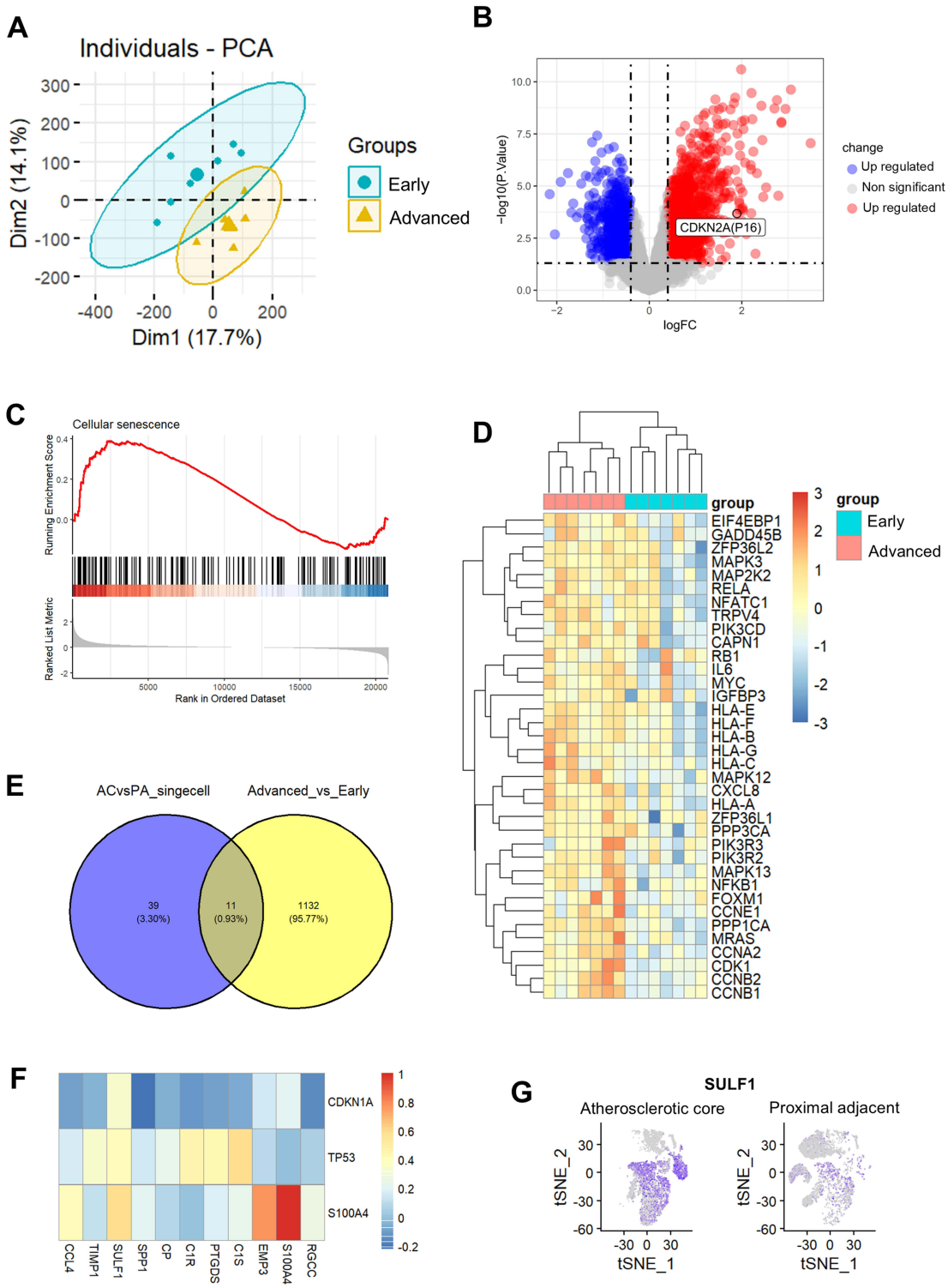

Figure 3 *SULF1* is a key gene affecting vascular EC senescence. (**A**) PCA plot displaying the degree of transcriptional difference of genes across the samples, where each point corresponds to a sample and the interpoint distances indicate the degree of similarity or dissimilarity in their gene expression profiles. (**B**) Differential gene expressions between two sample groups are illustrated in the volcano plot. The x-axis denotes the log-fold change in gene expression between groups, and the y-axis signifies the statistical significance of these differences. Points that diverge from the diagonal mark genes with significant differential expression, with upregulated genes located in the upper right quadrant and downregulated genes in the lower left quadrant. (**C**) The GSEA plot presents the outcomes of gene set enrichment analysis, where the x-axis shows the ranked list of genes based on their differential expression and the y-axis indicates the enrichment score for each gene set. (**D**) Heatmap displaying the expression levels of senescence-related genes across various samples, with the color intensity of each cell corresponding to the expression level of the corresponding gene in the corresponding sample. (**E**) The 50 genes most highly expressed in vascular ECs in the AC group relative to those in the PA group according to the single-cell data, as well as their intersection with genes differentially expressed between patients with late-stage sclerosis and those with early-stage disease, were identified. (**F**) Within the matrix, each cell represents the correlation coefficient between two variables, with warm colors representing positive correlations and cool colors indicating negative correlations. (**G**) t-SNE plot depicting the expression patterns of *SULF1* across different subgroups.

We conducted an analysis of the single-cell data of the top 50 genes most highly expressed in vascular ECs in the AC group compared with those in the PA group. Additionally, we examined the differential expressed genes (DEGs) between advanced atherosclerosis patients and those in the early stages. Given that the early-stage transcriptome represents a mixture of various tissues, not exclusively endothelial ones, we selected DEGs with a logFC > 0.4 and a p value < 0.05. Ultimately, we identified 11 key genes which are highly expressed in atherosclerotic tissue (Figure 3E). We further analyzed the correlation of these 11 genes with senescence markers to pinpoint those associated with senescence and discovered a positive correlation with *SULF1* expression (Figure 3F). Concurrently, single-cell analysis revealed high expression of *SULF1* in the vascular ECs of the AC group (Figure 3G). Furthermore, we also discovered that the expression of SULF1 shows differential regulation in fibroblasts and smooth muscle cells (Supplementary Figure 2).

Next, the EC subpopulations were classified into six clusters (Cluster 0–5) through constructing pseudotime trajectories, with a high *SULF1* expression in Cluster 2 (Figure 4A and B). Pseudotime trajectory analysis demonstrated that Cluster 3 served as the starting point, with one branch progressing toward Cluster 2 and another toward Cluster 0 (Figure 4C and D). Enrichment analysis indicated that Cluster 2 was associated with pathways such as TNF signaling, cellular senescence, and artery development, suggesting its significance in endothelial inflammatory and senescence (Figure 4E). The expression of *SULF1* at the terminal branch point in Cluster 2 further implied a potential link between this gene and cellular senescence (Figure 4F). To conclude, combined analysis of single-cell and bulk transcriptomic data revealed that *SULF1* is a potential gene affecting vascular endothelial senescence in the progression of atherosclerosis.

SULF1 is Related to EC Senescence Occurred in Atherosclerosis

To validate the authenticity of our bioinformatic analysis, we established an atherosclerosis model based on *ApoE*-null mice. Immunofluorescence staining revealed colocalization of CD31 (endothelial marker) and p53 (senescence marker) in plaque-surface endothelial cells, confirming the occurrence of EC senescence (Figure 5A and Supplementary Figure 3C). To rule out any potential influence of sex as a confounding variable, we repeated the experiments using female mice and obtained consistent results (Supplementary Figure 3A–B). Furthermore, HAECs treated with ox-LDL showed increased mRNA levels of senescence-related markers, including p16, p21, and p53 (Figure 5B–D). Correspondingly, the upregulation of these markers at the protein level was confirmed by Western blotting (Figure 5E–G).

Next, a comprehensive investigation was conducted to examine the expression profile of *SULF1* in ECs under atherosclerotic conditions. Compared with the vasculature of normal mice, the aortic ECs of atherosclerotic mice presented significant greater expression of *SULF1* (Figure 6A and B). To account for potential sex-related differences, the experiments were repeated in female mice, which yielded similar results (Supplementary Figure 4A–B). Western blot analysis of aortic tissues further confirmed the increased expression of *SULF1* in atherosclerotic tissues (Figure 6C and D). A marked increase in *SULF1* expression at both transcriptional and translational levels was detected in HAECs following ox-LDL treatment (Figure 6E–G). Collectively, these results demonstrated the upregulation of *SULF1* and occurrence of EC senescence in atherosclerotic models in vivo and in vitro, suggesting that *SULF1* might play a role in EC senescence during atherogenesis.

Knocking Down SULF1 Reversed Ox-LDL-Induced HAECs Senescence

To validate the association between *SULF1* and endothelial cell senescence, we performed siRNA-mediated *SULF1* silencing in HAECs, with knockdown efficiency verified through Western blotting and qPCR (Figure 7A and B). The upregulation of senescence-related markers (p16, p21, and p53) caused by ox-LDL exposure was significantly attenuated following SULF1 suppression, as evidenced by both qPCR and Western blot results (Figure 7C–H). Consistent with these findings, ox-LDL treatment markedly elevated the quantity of SA-β-gal-positive cells, whereas *SULF1* depletion substantially decreased this senescent cell population (Figure 7I and J). Cell migration capacity was examined using wound closure assays, revealing that ox-LDL-induced senescent HAECs exhibited impaired migratory ability compared to controls. Notably, *SULF1*-deficient cells displayed enhanced wound healing capacity relative to ox-LDL-treated counterparts (Figure 7K and L). Collectively, these data demonstrate that *SULF1* downregulation can counteract ox-LDL-triggered endothelial senescence, suggesting its therapeutic potential for atherosclerotic conditions.

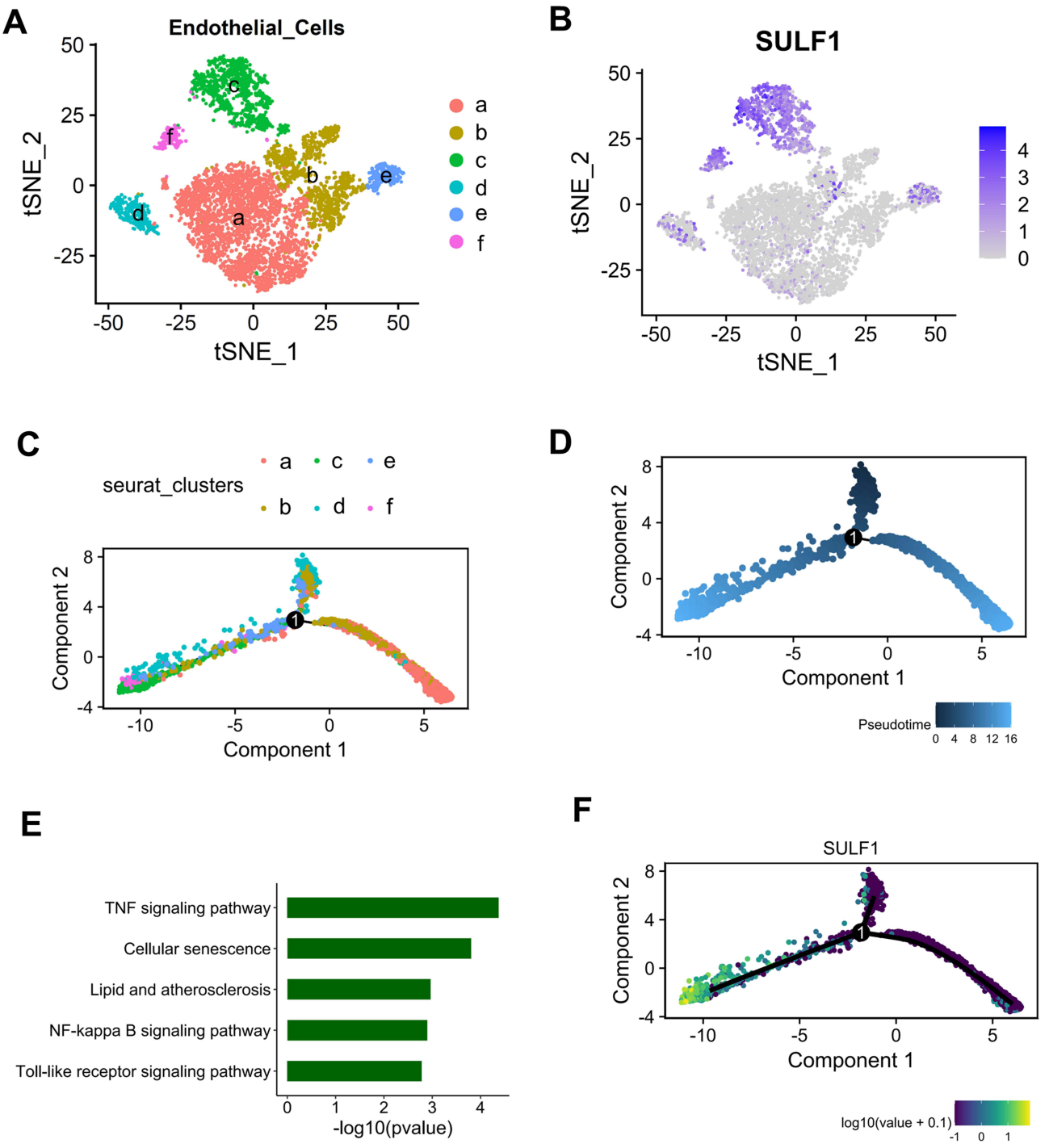

Figure 4 Pseudotime analysis of ECs. (**A**) ECs were classified into six clusters (0–5). (**B**) Examination revealed that *SULF1* was highly expressed in Cluster 2. (**C** and **D**) Pseudotime trajectory analysis demonstrated that Cluster 3 served as the starting point, with one branch progressing toward Cluster 2 and another toward Cluster 0. (**E**) Enrichment analysis indicated that Cluster 2 was associated with pathways such as TNF signaling, cellular senescence, and artery development. (**F**) *SULF1* was expressed at the terminal branch point in Cluster 2.

Discussion

Within the scope of atherosclerosis, our research investigated the complex dynamics of EC senescence via scRNA-seq and RNA-seq data. The findings herein elucidate the role of EC senescence within atherosclerotic plaques, which is highly important for deciphering disease progression.

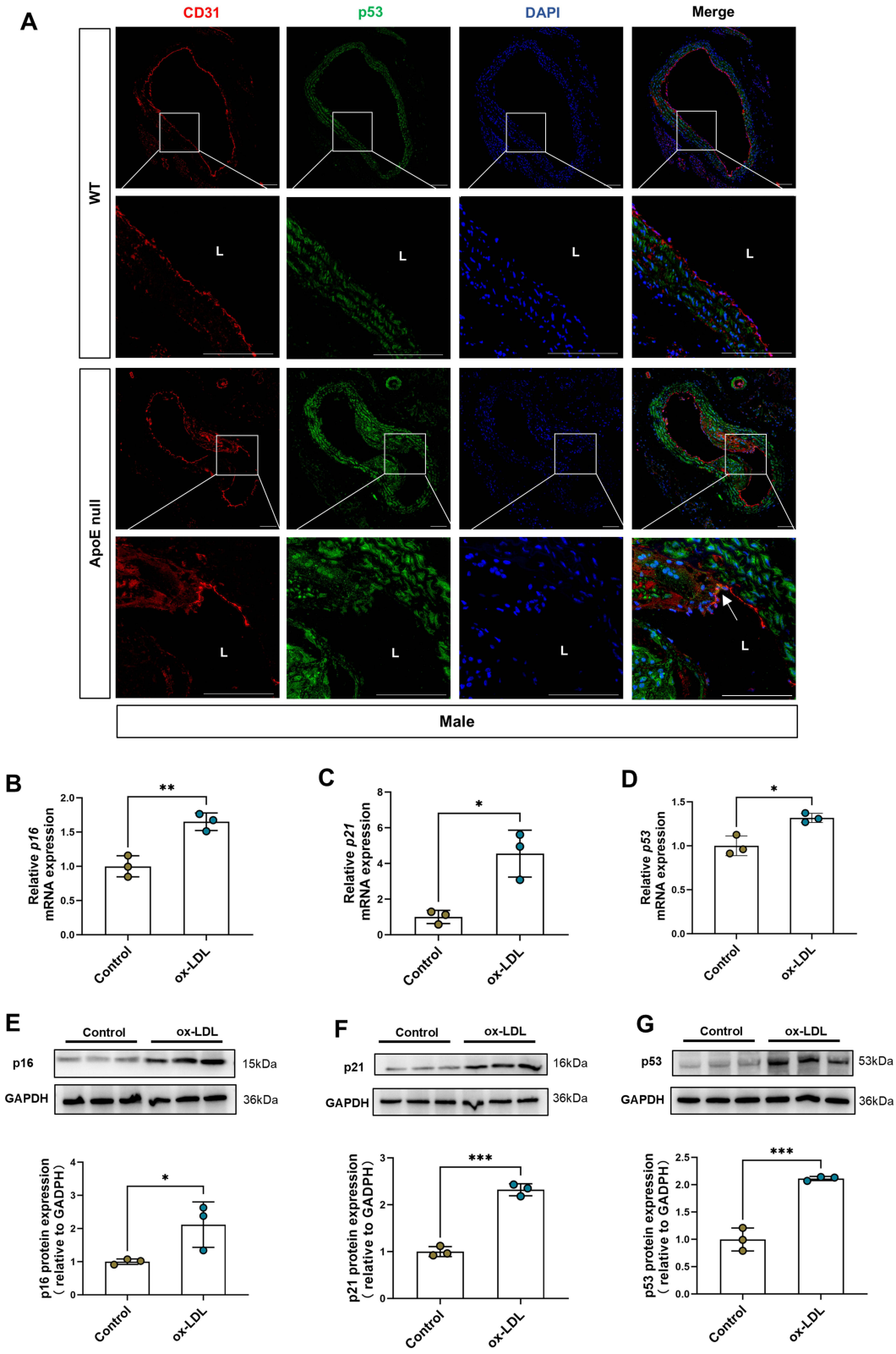

Figure 5 The senescence of ECs exists in atherosclerotic plaques. (**A**) Immunofluorescence staining revealed colocalization of CD31 and p53 in male mice (n = 6 independent biological replicates). (**B**–**D**) The mRNA levels of *p16, p21*, and *p53* in the HAECs treated with ox-LDL measured by RT-qPCR (n = 3 independent biological replicates). (**E**–**G**) Upregulation of these markers at the protein level was confirmed by Western blotting (n = 3 independent biological replicates). Scale bar = 100 μm. L: Lumen. White arrow: the co-localization signals of CD31 (red) and p53 (green). For all bar graphs, data are means ± SEM, **p* < 0.05, ***p* < 0.01, ****p* < 0.001 (determined by Student's *t*-test).

https://doi.org/10.2147/JIR.S544852

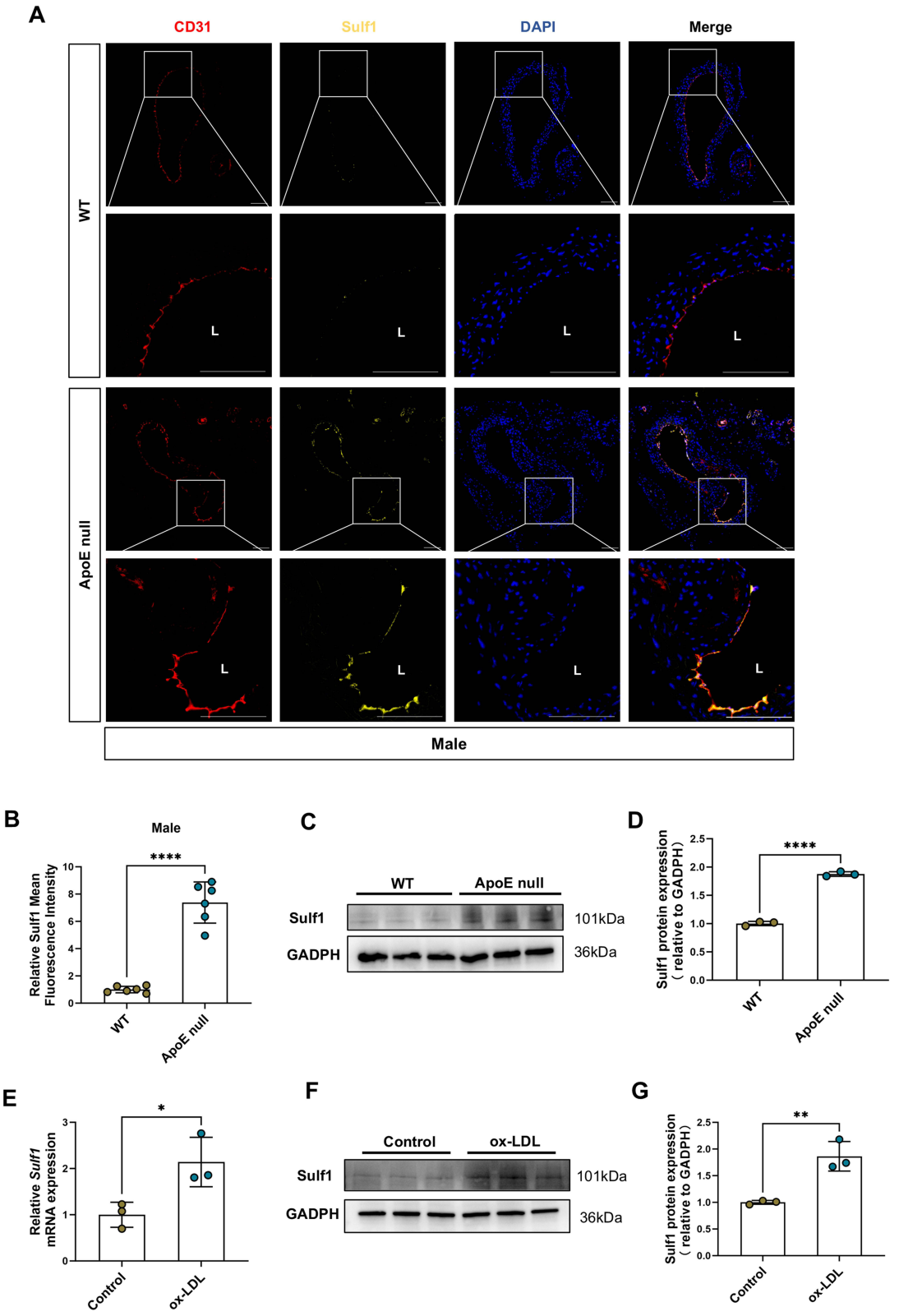

Figure 6 An increase in *SULF1* expression was observed in the ECs of atherosclerotic plaques. (**A** and **B**) Compared with the vasculature of normal mice, the aortic ECs of atherosclerotic mice presented significant greater expression of *Sulf1* in male mice (n = 6 independent biological replicates). (**C** and **D**) Western blot analysis of aortic tissues further confirmed the increased expression of *SULF1* in atherosclerotic tissues (n = 3 independent biological replicates). (**E**–**G**) A marked increase in *SULF1* expression at both transcriptional and translational levels was detected in HAECs treated with ox-LDL (n = 3 independent biological replicates). Scale bar = 100 μm. L: Lumen. For all bar graphs, data are means ± SEM, *$p < 0.05$, **$p < 0.01$, ****$p < 0.0001$ (determined by Student's *t*-test).

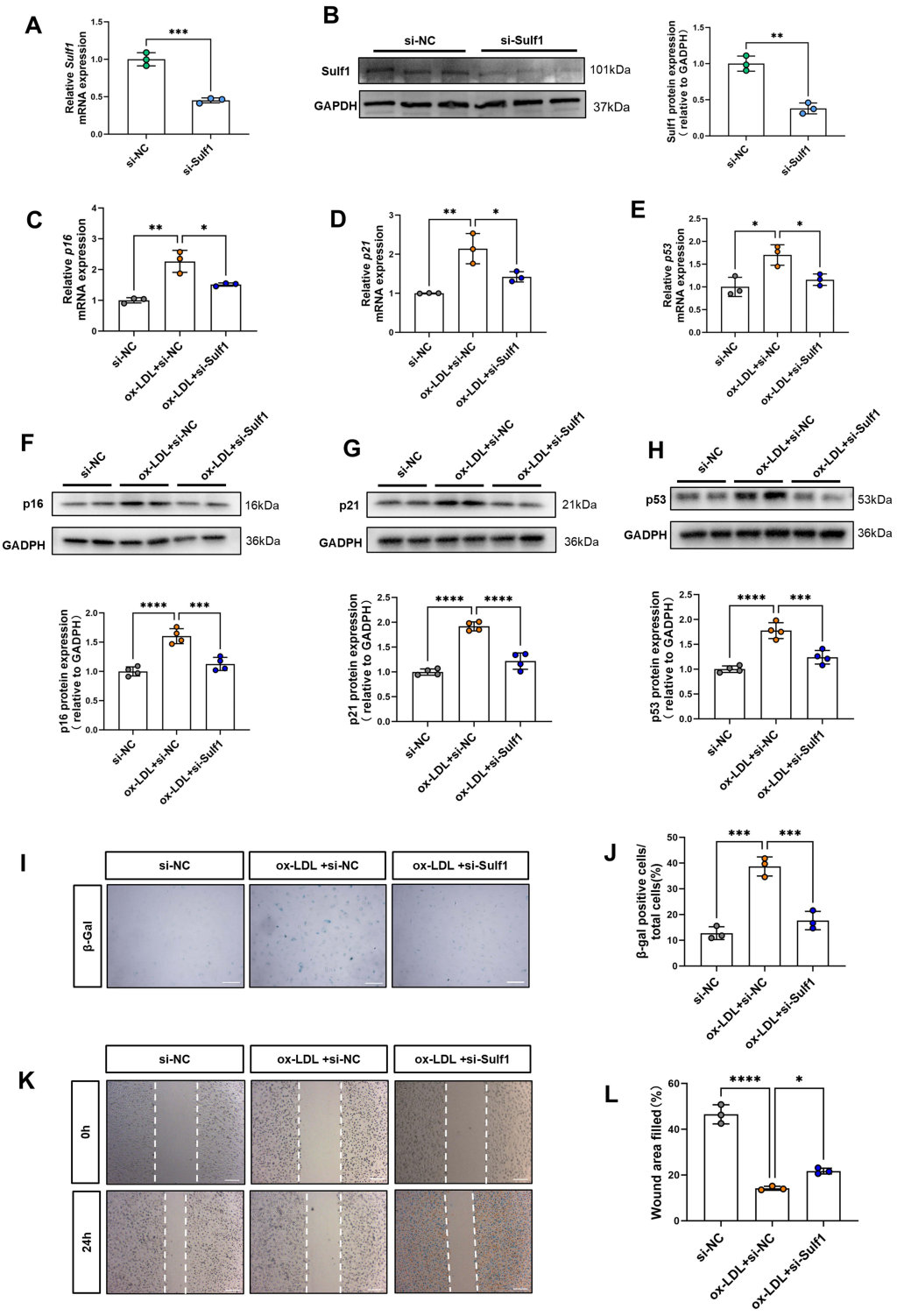

Figure 7 Knocking down *SULF1* reversed ox-LDL-induced aging in HAECs. (**A** and **B**) After siRNA was used to knock down *SULF1*, Western blotting and RT-qPCR were used to test the knockdown efficacy (n = 3 independent biological replicates). (**C**–**E**) After siRNA was used to knock down *SULF1*, RT-qPCR revealed that the expression of the aging markers p16, p21, and p53 in HAECs was lower than that in ox-LDL-induced HAECs (n = 3 independent biological replicates). (**F**–**H**) After siRNA was used to knock down *SULF1*, Western blot revealed that the expression of the aging markers p16, p21, and p53 in HAECs was lower than that in ox-LDL-induced HAECs (n = 4 independent biological replicates). (**I** and **J**) Knockdown of *SULF1* with siRNA led to a substantial reduction in the number of β-gal-positive cells (n = 3 independent biological replicates). (**K** and **L**) Wound healing tests revealed that the migration of cells in which *SULF1* was knocked down was markedly greater than that of the ox-LDL group (n = 3 independent biological replicates). Scale bar = 100 μm. β-gal, β-galactosidase. The dashed lines indicate the cell boundary. For all bar graphs, data are means ± SEM, *$p < 0.05$, **$p < 0.01$, ***$p < 0.001$, ****$p < 0.0001$ (determined by one-way ANOVA).

https://doi.org/10.2147/JIR.S544852

The present investigation revealed significantly increased expression of cellular senescence markers in ECs associated with atherosclerotic lesions. Current evidence indicates that endothelial senescence plays a pivotal role in atherogenesis, potentially representing one of the earliest pathogenic events in vascular plaque formation.[10,19,20] Senescent ECs demonstrate impaired nitric oxide synthesis and disrupted endothelial barrier integrity, primarily due to structural disarrangement of intercellular junctions including both adherens and tight junctions.[21] Hypercholesterolemia, a well-established risk factor for atherosclerosis, promotes the accumulation of ox-LDL within the subendothelial space. Importantly, the integrity of endothelial coverage over atherosclerotic plaques serves as a crucial determinant of plaque stability, with endothelial denudation predisposing to thrombotic complications at lesion sites.[22,23] Collectively, these findings establish endothelial senescence as a fundamental mechanism underlying both the initiation and progression of atherosclerotic vascular disease.

We identified *SULF1* as a key contributor to endothelial senescence and experimentally demonstrated that down-regulation of *TREM-1* reversed endothelial senescence. *SULF1*, a heparan sulfate 6-O-endosulfatase, plays a critical role in endothelial senescence by modulating growth factor signaling, oxidative stress, inflammatory responses and telomere maintenance. Through its regulation of heparan sulfate proteoglycans (HSPGs), *SULF1* influences the bioavailability of key growth factors, such as VEGF and FGF, which are essential for ECs survival and angiogenesis.[13,24–26] The ability of *SULF1* to fine-tune these signaling pathways suggests its potential role in mitigating senescence by maintaining growth factor homeostasis. Oxidative stress represents a principal contributor to endothelial senescence, manifesting through elevated reactive oxygen species (ROS) accumulation and genomic instability.[27] *SULF1* may exert indirect regulatory effects on oxidative stress by modifying the accessibility of antioxidant compounds and ROS-detoxifying enzymes via HSPG modulation. Specifically, *SULF1*-dependent HSPG alterations could influence enzymatic activities including superoxide dismutase (SOD) and NADPH oxidase systems, consequently impacting cellular redox balance.[28] Additional investigations are required to delineate the precise mechanistic relationship between *SULF1* and oxidative stress mechanisms in endothelial cells. Persistent inflammatory activation constitutes a hallmark characteristic of senescent endothelium, primarily driven by senescence-associated secretory phenotype (SASP) factors. Emerging evidence suggests *SULF1* participates in inflammatory regulation by controlling the mobilization of HSPG-bound signaling molecules.[29,30] Notably, *SULF1*-mediated processes may limit the biological activity of inflammatory mediators including IL-6 and TNF-α, potentially ameliorating the pro-inflammatory microenvironment associated with endothelial impairment.[31,32] These anti-inflammatory properties highlight *SULF1*'s potential as an intervention target for inflammation-related senescence pathways. While direct evidence linking *SULF1* to telomere biology is limited, its role in growth factor signaling and oxidative stress regulation suggests potential indirect effects on telomere integrity. For example, *SULF1*-mediated promotion of VEGF signaling increases telomerase activity, thereby delaying replicative senescence.[24] Future studies should investigate whether *SULF1* directly influences telomere length or telomerase activity in ECs.

Furthermore, while this study has focused on the role of *SULF1* in endothelial cell senescence, our preliminary bioinformatic analysis of single-cell data suggests that *SULF1* expression is also differentially regulated in fibroblasts and smooth muscle cells between atherosclerotic and control groups. This intriguing observation warrants further investigation to elucidate the cell-type-specific functions of *SULF1* in the complex pathophysiology of atherosclerosis. Despite the growing interest in *SULF1*, several questions remain unanswered, including how *SULF1* expression changes with age and the specific molecular mechanisms underlying its effects on endothelial senescence. Additionally, the interplay between *SULF1* and other senescence regulators, such as *SIRT1* and *KLF4*, warrants further investigation. Advanced techniques, including single-cell omics and CRISPR-based gene editing, may provide deeper insights into the role of *SULF1* in endothelial biology. Furthermore, while our loss-of-function (knockdown) experiments suggest a contributory role, the absence of gain-of-function (overexpression) data means that we cannot conclusively state that *SULF1* is a primary driver, rather than a secondary consequence, of the senescent phenotype. Future studies employing *SULF1* overexpression models are warranted to solidify this causal link.

Conclusion

Combining scRNA-seq and RNA-seq data analysis, the present study identified *SULF1* as a gene potentially associated with endothelial senescence. Our in vitro experiments demonstrated that *SULF1* expression correlates with senescence markers in endothelial cells under atherosclerotic conditions. These findings suggest a possible role of *SULF1* in atherosclerosis progression through endothelial senescence pathways. Further studies, particularly in vivo functional validations, are warranted to fully establish the therapeutic potential of *SULF1* in atherosclerosis management.

Author Contributions

All authors made a significant contribution to the work reported, whether that is in the conception, study design, execution, acquisition of data, analysis and interpretation, or in all these areas; took part in drafting, revising, or critically reviewing the article; gave final approval of the version to be published; have agreed on the journal to which the article has been submitted; and agree to be accountable for all aspects of the work.

Funding

This work was supported in part by the National Natural Science Foundation of China (82400541, 82120108004, 91539118, 81611130092), the Postdoctoral Fellowship Program of CPSF under grant number GZC20242284, the National Talent Support Project of Daping Hospital (2025RCTJC09), Shanghai foundation Grant for supporting the military and families (E3F2A20102) and the Program of EnShi TuJia and Miao Autonomous Prefecture Bureau of Scientific and Technological Affairs.

Disclosure

All authors declare that they have no competing interests.

References

1. Tsao CW, Aday AW, Almarzooq ZI, et al. Heart disease and stroke statistics-2023 update: a report from the American heart association. *Circulation*. 2023;147(8):e93–e621. doi:10.1161/CIR.0000000000001123
2. Dai H, Much AA, Maor E, et al. Global, regional, and national burden of ischaemic heart disease and i ts attributable risk factors, 1990-2017: results from the global burden of disease study 2017. *Eur Heart J Qual Care Clin Outcomes*. 2022;8(1):50–60. doi:10.1093/ehjqcco/qcaa076
3. Libby P, Buring JE, Badimon L, et al. Atherosclerosis. *Nat Rev Dis Primers*. 2019;5(1):56. doi:10.1038/s41572-019-0106-z
4. Wang X, Shen Y, Shang M, Liu X, Munn LL. Endothelial mechanobiology in atherosclerosis. *Cardiovasc Res*. 2023;119(8):1656–1675. doi:10.1093/cvr/cvad076
5. Gimbrone MA, García-Cardeña G. Endothelial cell dysfunction and the pathobiology of atherosclerosis. *Circulation Res*. 2016;118(4):620–636. doi:10.1161/CIRCRESAHA.115.306301
6. Dou F, Wu B, Chen J, et al. PPARα targeting GDF11 inhibits vascular endothelial cell senescence in an atherosclerosis model. *Oxid Med Cell Longev*. 2021;2021(1):2045259. doi:10.1155/2021/2045259
7. You Y, Chen X, Chen Y, et al. Epigenetic modulation of Drp1-mediated mitochondrial fission by inhibition of S-adenosylhomocysteine hydrolase promotes vascular senescence and atherosclerosis. *Redox Biol*. 2023;65:102828. doi:10.1016/j.redox.2023.102828
8. Dong M, Chen M, Zhang Y, et al. Oscillatory shear stress promotes endothelial senescence and atheroscl erosis via STING activation. *Biochem Biophys Res Commun*. 2024;715:149979. doi:10.1016/j.bbrc.2024.149979
9. Wu C-M, Zheng L, Wang Q, Hu Y-W. The emerging role of cell senescence in atherosclerosis. *Clin Chem Lab Med*. 2021;59(1):27–38. doi:10.1515/cclm-2020-0601
10. Bu -L-L, Yuan -H-H, Xie -L-L, et al. New dawn for atherosclerosis: vascular endothelial cell senescence and death. *Int J Mol Sci*. 2023;24 (20):15160. doi:10.3390/ijms242015160
11. Bloom SI, Islam MT, Lesniewski LA, Donato AJ. Mechanisms and consequences of endothelial cell senescence. *Nat Rev Cardiol*. 2023;20:38–51. doi:10.1038/s41569-022-00739-0
12. Nishitsuji K. Heparan sulfate S-domains and extracellular sulfatases (Sulfs): their possible roles in protein aggregation diseases. *Glycoconjugate J*. 2018;35(4):387–396. doi:10.1007/s10719-018-9833-8
13. Han M, Zhu H, Chen X, Luo X. 6-O-endosulfatases in tumor metastasis: heparan sulfate proteoglycans modification and potential therapeutic targets. *Am J Cancer Res*. 2024;14(2):897–916. doi:10.62347/rxve7097
14. Pham TP, van Bergen AS, Kremer V, et al. LncRNA AERRIE is required for sulfatase 1 expression, but not for endothelial-to-mesenchymal transition. *Int J Mol Sci*. 2021;22(15):8088. doi:10.3390/ijms22158088
15. Tan J, Liang Y, Yang Z, et al. Single-cell transcriptomics reveals crucial cell subsets and functional heterogeneity associated with carotid atherosclerosis and cerebrovascular events. *Arterioscler Thromb Vasc Biol*. 2023;43(12):2312–2332. doi:10.1161/atvbaha.123.318974
16. Alsaigh T, Evans D, Frankel D, Torkamani A. Decoding the transcriptome of calcified atherosclerotic plaque at single-cell resolution. *Commun Biol*. 2022;5(1):1084. doi:10.1038/s42003-022-04056-7

17. Döring Y, Manthey HD, Drechsler M, et al. Auto-antigenic protein-DNA complexes stimulate plasmacytoid dendritic cells to promote atherosclerosis. *Circulation*. 2012;125(13):1673–1683. doi:10.1161/circulationaha.111.046755
18. Qiu X, Hill A, Packer J, et al. Single-cell mRNA quantification and differential analysis with Census. *Nat Methods*. 2017;14(3):309–315. doi:10.1038/nmeth.4150
19. Hwang HJ, Kim N, Herman AB, Gorospe M, Lee JS. Factors and pathways modulating endothelial cell senescence in vascular aging. *Int J Mol Sci*. 2022;23(17):10135. doi:10.3390/ijms231710135
20. Tian XL, Li Y. Endothelial cell senescence and age-related vascular diseases. *J Genet Genomics*. 2014;41(9):485–495. doi:10.1016/j.jgg.2014.08.001
21. Krouwer VJ, Hekking LH, Langelaar-Makkinje M, Regan-Klapisz E, Post JA. Endothelial cell senescence is associated with disrupted cell-cell junctions and increased monolayer permeability. *Vasc Cell*. 2012;4(1):12. doi:10.1186/2045-824x-4-12
22. Libby P. Seeing and sampling the surface of the atherosclerotic plaque: red or white can make blue. *Arterioscler Thromb Vasc Biol*. 2016;36(12):2275–2277. doi:10.1161/atvbaha.116.308491
23. Molinaro R, Yu M, Sausen G, et al. Targeted delivery of protein arginine deiminase-4 inhibitors to limit arterial intimal NETosis and preserve endothelial integrity. *Cardiovasc Res*. 2021;117(13):2652–2663. doi:10.1093/cvr/cvab074
24. Grunewald M, Kumar S, Sharife H, et al. Counteracting age-related VEGF signaling insufficiency promotes healthy aging and extends life span. *Science*. 2021;373(6554). doi:10.1126/science.abc8479
25. Wang H, Chen J, Chen X, et al. Cancer-associated fibroblasts expressing sulfatase 1 facilitate VEGFA-dependent microenvironmental remodeling to support colorectal cancer. *Cancer Res*. 2024;84(20):3371–3387. doi:10.1158/0008-5472.Can-23-3987
26. Korf-Klingebiel M, Reboll MR, Grote K, et al. Heparan sulfate-editing extracellular sulfatases enhance VEGF bioavailability for ischemic heart repair. *Circ Res*. 2019;125(9):787–801. doi:10.1161/circresaha.119.315023
27. Hajam YA, Rani R, Ganie SY, et al. Oxidative stress in human pathology and aging: molecular mechanisms and perspectives. *Cells*. 2022;11(3):552. doi:10.3390/cells11030552
28. Ishisaka A, Ichikawa S, Sakakibara H, et al. Accumulation of orally administered quercetin in brain tissue and its antioxidative effects in rats. *Free Radic Biol Med*. 2011;51(7):1329–1336. doi:10.1016/j.freeradbiomed.2011.06.017
29. Oshima K, Han X, Ouyang Y, et al. Loss of endothelial sulfatase-1 after experimental sepsis attenuates subsequent pulmonary inflammatory responses. *Am J Physiol Lung Cell Mol Physiol*. 2019;317(5):L667–l677. doi:10.1152/ajplung.00175.2019
30. Gill RM, Michael A, Westley L, et al. SULF1/SULF2 splice variants differentially regulate pancreatic tumour growth progression. *Exp Cell Res*. 2014;324(2):157–171. doi:10.1016/j.yexcr.2014.04.001
31. Tsai TT, Ho NY, Fang HC, et al. Increased sulfatase 1 gene expression in degenerative intervertebral disc cells. *J Orthop Res*. 2015;33(3):312–317. doi:10.1002/jor.22766
32. Sikora AS, Hellec C, Carpentier M, et al. Tumour-necrosis factor-α induces heparan sulfate 6-O-endosulfatase 1 (Sulf-1) expression in fibroblasts. *Int J Biochem Cell Biol*. 2016;80:57–65. doi:10.1016/j.biocel.2016.09.021